ANL-7670

PROPERTY OF
ANL-W Technical Library

Argonne National Laboratory

MATERIALS-COOLANT INTERACTIONS IN EBR-II

by

W. E. Ruther, T. D. Claar,
S. Greenberg, and R. V. Strain

The facilities of Argonne National Laboratory are owned by the United States Government. Under the terms of a contract (W-31-109-Eng-38) between the U. S. Atomic Energy Commission, Argonne Universities Association and The University of Chicago, the University employs the staff and operates the Laboratory in accordance with policies and programs formulated, approved and reviewed by the Association.

MEMBERS OF ARGONNE UNIVERSITIES ASSOCIATION

The University of Arizona
Carnegie-Mellon University
Case Western Reserve University
The University of Chicago
University of Cincinnati
Illinois Institute of Technology
University of Illinois
Indiana University
Iowa State University
The University of Iowa
Kansas State University
The University of Kansas
Loyola University
Marquette University
Michigan State University
The University of Michigan
University of Minnesota
University of Missouri
Northwestern University
University of Notre Dame
The Ohio State University
Ohio University
The Pennsylvania State University
Purdue University
Saint Louis University
Southern Illinois University
University of Texas
Washington University
Wayne State University
The University of Wisconsin

LEGAL NOTICE

This report was prepared as an account of Government sponsored work. Neither the United States, nor the Commission, nor any person acting on behalf of the Commission:

A. Makes any warranty or representation, expressed or implied, with respect to the accuracy, completeness, or usefulness of the information contained in this report, or that the use of any information, apparatus, method, or process disclosed in this report may not infringe privately owned rights; or

B. Assumes any liabilities with respect to the use of, or for damages resulting from the use of any information, apparatus, method, or process disclosed in this report.

As used in the above, "person acting on behalf of the Commission" includes any employee or contractor of the Commission, or employee of such contractor, to the extent that such employee or contractor of the Commission, or employee of such contractor prepares, disseminates, or provides access to, any information pursuant to his employment or contract with the Commission, or his employment with such contractor.

Printed in the United States of America
Available from
Clearinghouse for Federal Scientific and Technical Information
National Bureau of Standards, U. S. Department of Commerce
Springfield, Virginia 22151
Price: Printed Copy $3.00; Microfiche $0.65

ANL-7670
Reactor Technology

ARGONNE NATIONAL LABORATORY
9700 South Cass Avenue
Argonne, Illinois 60439

MATERIALS-COOLANT INTERACTIONS IN EBR-II

by

W. E. Ruther, T. D. Claar,
S. Greenberg, and R. V. Strain

EBR-II Project

March 1970

TABLE OF CONTENTS

	Page
ABSTRACT	7
I. INTRODUCTION	7
II. EXPERIMENTAL PROCEDURE	9
III. DATA AND RESULTS	10
A. Direct-compatibility Problems	10
1. Partial Dissolution of a Copper Bus Bar	10
2. Wear Corrosion of Beryllium-Copper Bushing Rings	13
3. Bismuth-Tin Incident	14
4. Tantalum Corrosion Product	17
B. Failures	17
1. Apparent Cracking of Type 304L Stainless Steel Fuel-element Cladding	17
2. Failure of Type 347 Stainless Steel Valve Bellows	20
3. Failure of Inconel-600 Rupture Disc	21
4. Fracture of Type 420 Stainless Steel Roll Pin	23
C. Examination of Components	24
1. Type 304 L Stainless Steel Fuel Cladding	24
2. Type 304 Stainless Steel Guide Thimbles	29
3. Gripper Assembly from Control-rod Driver Number 6	32
4. Type 304 Stainless Steel Piping (Secondary Sodium System)	34
D. Evaluations of In-reactor Corrosion	38
1. Spool Specimens	38
2. Nickel Subassembly	43
IV. DISCUSSION	44
A. Components	44
B. Corrosion Evaluations	45
ACKNOWLEDGMENTS	46
REFERENCES	47

LIST OF FIGURES

No.	Title	Page
1.	Schematic Representation of EBR-II Primary and Secondary Sodium Systems	9
2.	Copper Deposits on ID of Inner Tube of EBR-II Heat Exchanger Etched Electrolytically in 10% Oxalic Acid	11
3.	Copper Transfer Loop	12
4.	Section of Type 304 Stainless Steel Tubing, Etched Electrolytically in 10% Oxalic Acid, Taken from 965-1000°F Region of Copper Transfer Loop	12
5.	Cross Section of Berylco-25 Bushing from Top Set of Control-rod Subassembly L-435 after 10,000 hr in Reactor Grid	13
6.	Microstructures of Berylco-25 Alloy before and after Exposure in EBR-II	15
7.	Bushing Materials after EBR-II Exposure in Control-rod Subassembly L-457 for ~5500 hr	16
8.	Cladding of Element C-249-16 after 45-sec Etching in 5% Oxalic Acid	18
9.	Type 304L Stainless Steel Tubing That Had Been Streaked with Apiezon-N Grease and Exposed to 1022°F Sodium for One week after a 45-sec Etching in 5% Oxalic Acid	19
10.	Transverse Section of Bellows of SN-17 Valve after 10-sec Etching in 5% Oxalic Acid Showing Penetrating Fingers of Sodium Corrosion Product at Highly Stressed Region	20
11.	As-polished Transverse Section of the Corroded Network Showing Cracks and Missing Grains Adjacent to Perforated Area in Inconel-600 Rupture Disc	22
12.	Inner Surface of Failed Roll Pin Examined at Idaho	23
13.	Typical Microstructure of Type-420 Stainless Steel Roll Pins after 10-sec Etching in Glyceregia	24
14.	Irradiated Cladding Microstructure of Element 63--Subassembly C-2186S as a Function of Position	26
15.	Transverse Sections of Irradiated Cladding from Element 41--Subassembly C-278 after Etching in 10% Oxalic Acid Showing Sensitization at Both Surfaces	27
16.	Microstructures of As-received Cladding after Vacuum Heat Treatment at 1100°F and Etching in 10% Oxalic Acid	28

LIST OF FIGURES

No.	Title	Page
17.	Lack of Corrosive Effect of Sodium-removal Treatment or Storage on Irradiated Cladding	29
18.	Corrosion Interface for Specimen H14 after 15-sec Etching in 5% Oxalic Acid	30
19.	Corrosion Interface for Specimen H12 after 15-sec Etching in 5% Oxalic Acid	31
20.	Corrosion Interface for Specimen H7 after 15-sec Etching in 5% Oxalic Acid	31
21.	As-polished Stellite Clamp Gripper	33
22.	As-polished Outer Surface of Jaw Gripper Showing Thick Chromium Plating	33
23.	Compositional Zone at Unplated Surface of Jaw Gripper after 10-sec Etching in Warm 10% Nital	34
24.	As-polished Inner (Sodium) Surface of Secondary System Pipe	35
25.	As-polished Outer (Air) Surface of Secondary System Pipe	36
26.	Deposit on As-polished Inner (Sodium) Surface of Pipe	36
27.	Inner (Sodium) Surface after Electrolytic Etching by 5% Oxalic Acid for 45 sec	37
28.	EBR-II Corrosion Samples	39

LIST OF TABLES

No.	Title	Page
I.	Materials Originally in Contact with Liquid Sodium in EBR-II Primary System	8
II.	Impurity Levels in EBR-II Sodium	10
III.	Specimens from Safety-rod Guide Thimble	30
IV.	Chemical Analyses of Type 304 Stainless Steel Pipe after Sodium Exposure	37
V.	Composition of Vanadium-base Alloys	39
VI.	Composition of High-temperature Alloys	39
VII.	Sodium-exposure Data	40
VIII.	Weight-change Data for Vanadium Alloys	40
IX.	Weight-change Data for High-temperature Alloys	41
X.	Weight Loss of Nickel-200 Rings Exposed 2910 MWd in Position 7F5	43

MATERIALS-COOLANT INTERACTIONS IN EBR-II

by

W. E. Ruther, T. D. Claar,
S. Greenberg, and R. V. Strain

ABSTRACT

Of the many materials deliberately exposed to the EBR-II sodium coolant, only copper, beryllium copper, and tantalum experienced an undesirable direct reaction.

Failures of thin sections of normally resistant metals (Types 304, 347, and 420 stainless steels and Inconel) were related to the presence of a contaminant (carbonaceous material or oxide) on the surface before insertion into the reactor sodium.

Components removed from the reactor after long exposures showed only minor dissolution attack. The attack was greater with increasing temperature; however, radiation did not cause a detectable increase in the attack. Carbon transport among steels of differing carbon activity was inconsequential.

Quantitative corrosion evaluations of vanadium alloys, stainless steels, nickel, and nickel-base alloys in the reactor coolant showed rapid corrosive attack only for unalloyed vanadium.

I. INTRODUCTION

The sodium-cooled Experimental Breeder Reactor II (EBR-II) was conceived and designed as a demonstration plant to show the feasibility of a self-contained facility that combines electrical power generation with nuclear breeding and fuel reprocessing. Subassemblies for a long-range materials-surveillance program were placed in the reactor before startup. However, little effort beyond solving immediate problems could be spared for materials evaluation while the EBR-II was attaining its primary goals. Since the demonstration period has been successfully completed, the role of the EBR-II in the LMFBR program has expanded to include a

closer scrutiny of materials-coolant interactions in addition to its main function as an irradiation test facility. The results of the examination of the first materials-test subassembly have been reported.[1]

Although other information, useful in the design and operation of a sodium-cooled reactor, has accumulated over the years of operation, much of it is contained in internal communications and is only briefly summarized in progress reports. In this form, it is largely inaccessible to interested persons outside the EBR-II Project. The present report remedies this situation by discussing essentially all the reactor-compatibility problems and materials-evaluation data obtained to date, so that they will be readily available to other organizations.

Types 304 and 304L stainless steel predominate as the metal surfaces in contact with the sodium coolant of the EBR-II. However, where some special property has been required, other types of materials have been used, and these are listed in Table I. Most of these materials, chosen over ten years ago, have been satisfactory. In a few instances, however, direct compatibility problems with the sodium coolant have arisen. Such problems are the subject of Section III.A of this report.

TABLE I. Materials Originally in Contact with Liquid Sodium in EBR-II Primary System

Material	Approximate Sodium Temperatures, °F
Alloy Steel, SAE 4340	700
Aluminum Bronze (Ampco 18-13)	700, 800-850, 900
Aluminum Bronze (Ampco 18-23)	700
Beryllium Copper (Berylco 25)	700
Borated (1-1/2%) Type 304 Stainless Steel	700
Carbon Steel, ASTM 325-55T	700
Chromium-plated Types 304, 410, and 420 Stainless Steel	700 and 900
Colmonoy 4 and 5	900
Copper	700
Inconel	700
Inconel X	700
Monel	700
Nickel	700
Stainless Steel Types 303, 304, 316, 321, and 347	300 to ~1000
Stainless Steel Types 410 and 420	700 and 900
Stellite No. 3 and 6B	700 and 900
Tantalum	700
Tool Steel Types 18-4-1, 18-4-2, and Rex AA	700 and 900

In several instances, the material of construction was normally compatible with sodium, but exposure of thin sections to an unexpected contaminant resulted in component failure. Analyses of these failures are presented in Section II; examinations of representative components removed from the reactor comprise Section III of this report; Section IV discusses two sets of in-reactor corrosion evaluation experiments.

Wide ranges of materials, circumstances, and evaluation techniques are involved. For this reason, each examination is reported as a self-contained unit consisting of the history of the incident or material, the results of the investigation, and the conclusions.

II. EXPERIMENTAL PROCEDURE

Figure 1 is a schematic diagram of the pertinent components of the two EBR-II sodium systems. The reactor itself is cooled by primary-system sodium that enters at 700°F and emerges at approximately 900°F. The added heat is given up to a secondary sodium cooling system through the intermediate heat exchanger. Each sodium system has provisions for maintaining its sodium quality by cold-trapping impurities.

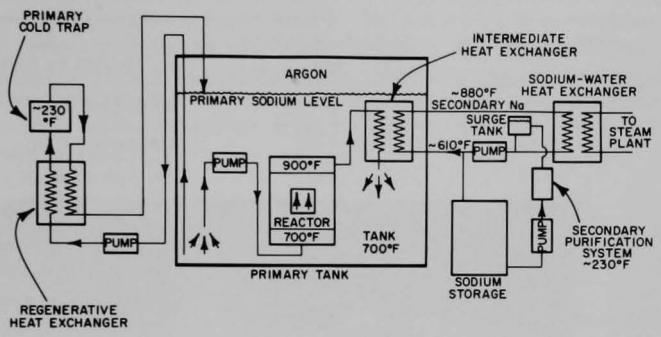

Fig. 1. Schematic Representation of EBR-II Primary and Secondary Sodium Systems. Neg. No. 52343.

Systematic chemical analyses of the sodium and plugging temperature measurements are used to monitor the quality of the sodium.

Initially, the Primary Sodium Purification System was operated only if the plugging temperature rose above 300°F. More recently, the primary purification system has been operated continuously with the trap at about 240°F. Table II lists typical values for the impurities present in EBR-II sodium; in general, all impurity levels are low.

Subassemblies within the primary reactor tank are subjected to a sodium-removal operation before they are exposed to air for dismantling. Approximately 25 g of sodium clings to surfaces within a subassembly after it has been removed from the reactor. This sodium is removed in a transfer cask at a station between the reactor and the Fuel Cycle Facility (FCF) air cell. During the transfer of the subassembly in the shielded cask from the reactor to the FCF, 30 cfm of argon is circulated through the subassembly to remove gamma-induced heat and to prevent the fuel and cladding from melting. The sodium-removal operation starts by introducing humidified air (air bubbled through water) at a rate of 0.4 cfm to the recirculating argon. The amount of humidified air available to oxidize the sodium is gradually increased by continuing to add humidified air to the recirculating argon for 15 min while removing the gas mixture

at a rate of 0.4 cfm. The rate of humidified air flow is then raised to 7 cfm for 15-30 min. At the end of this period the recirculating argon flow is stopped, and the subassembly is rinsed by flowing purified water up through it at a rate of 5 gal/min for 5 min. Passing dry air through the subassembly at 30 cfm for 60 min completes the sodium-removal operation. All items removed from the secondary system are washed in ethyl alcohol and rinsed in distilled water.

TABLE II. Impurity Levels[a] in EBR-II Sodium

Element	Primary System, ppm	Secondary System, ppm	Method of Analysis
O[b]	2-5	2-5	Amalgamation[2]
C	1-2	1-2	Oxyacidic flux[3]
H	1-2	1-2	Isotope dilution[4]
Al	<0.6	<0.6	Atomic-absorption spectrophotometry following vacuum distillation from a tantalum crucible
Bi	2	<0.1	
Ca	~0.05	<0.01	
Co	<0.04	<0.02	
Cr	0.03	0.03	
Cu	0.02	0.02	
Fe	0.06-0.1	0.1	
Mg	0.01-0.06	0.02	
Mn	<0.005	~0.005	
Mo	<0.07	<0.07	
Ni	<0.05	<0.05	
Pb	10-12	0.7	
Sn	20-25	<0.5	

[a]Recent analyses: September-December 1969.
[b]Plugging-temperature measurements indicate an oxygen content of $\lesssim 1$ ppm.

III. DATA AND RESULTS

A. Direct-compatibility Problems

Direct-compatibility problems are of four types, as discussed here.

1. Partial Dissolution of a Copper Bus Bar

In March 1967, after several years of satisfactory operation, sodium flow could not be established through a small auxiliary loop that contained the plugging-temperature valve assembly of the Primary Sodium Purification System. Inspection of the valve and the regenerative heat exchanger revealed deposits of metallic copper, and the exposed ends of the bus bars in the primary circuit auxiliary pump were identified as the source of the copper. Cladding the bus bars with stainless steel eliminated the source of copper, and continuous operation of the cold trap brought the

copper concentration in the sodium down to a level of ~0.1 ppm. As a further precaution, Monel and nickel transition members in the pump structure were also removed.

Interactions of copper and stainless steel in sodium were studied to ensure that no permanent damage had occurred to the stainless steel parts of the reactor. Seven sections of the regenerative heat exchanger in which the copper deposit had been noted were nickel plated to retain the copper, and these sections were examined metallographically. As shown in Fig. 2, the copper was in the form of a discontinuous deposit with poor adherence to the stainless steel surfaces; no microscopic evidence of interaction with the stainless steel was noted. Quantitative information obtained with the electron-beam microprobe substantiated that no penetration of the stainless steel by copper had occurred, not even along grain boundaries.

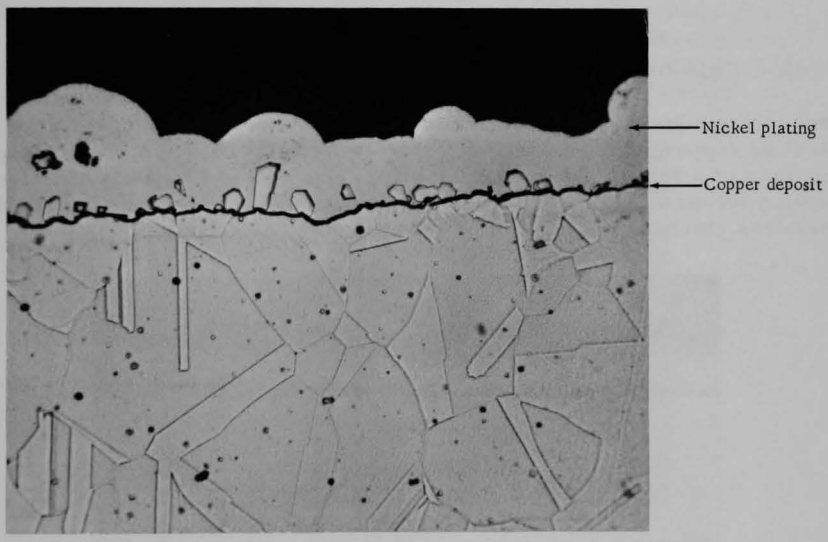

Fig. 2. Copper Deposits on ID of Inner Tube of EBR-II Heat Exchanger Etched Electrolytically in 10% Oxalic Acid. Mag. 500X. Neg. No. 47126.

These results were encouraging; however, since the temperatures in the heat exchanger were less than 700°F, additional high-temperature tests had to be made to ensure the integrity of the fuel-element cladding that operated at temperatures as high as 950°F. As might be expected from the temperature dependence of the copper solubility in sodium (log S varies inversely as 1/T, there was no evidence of a copper surface deposit on fuel elements removed from the reactor.

The small pumped loop shown in Fig. 3 was improvised from 0.495-in.-OD Type 304 stainless steel tubing. The temperature of the sodium was increased in the upper heater section from ~330°F at the pump to 1000°F in the loop. The sodium then passed over a copper source at 4.2 liters/hr and subsequently was cooled to 330°F in the lower portion of the apparatus. During the 10 days of testing, 4 g of copper were transferred from the source to the cooler portions of the loop.

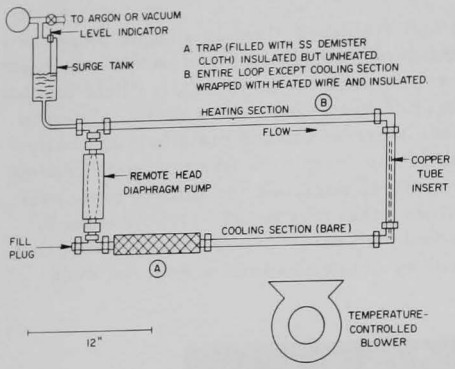

Fig. 3. Copper Transfer Loop. Neg. No. 51839.

Representative pieces of the loop tubing were examined metallographically, with particular emphasis on the higher-temperature sections. The copper-stainless steel interfaces were smooth, and no evidence of selective penetration of the stainless steel by copper was seen on any of the specimens. Figure 4 shows a typical example of a section exposed at 965-1000°F. When examined by the electron-beam microprobe, the same specimen showed no copper intrusion into the stainless steel.

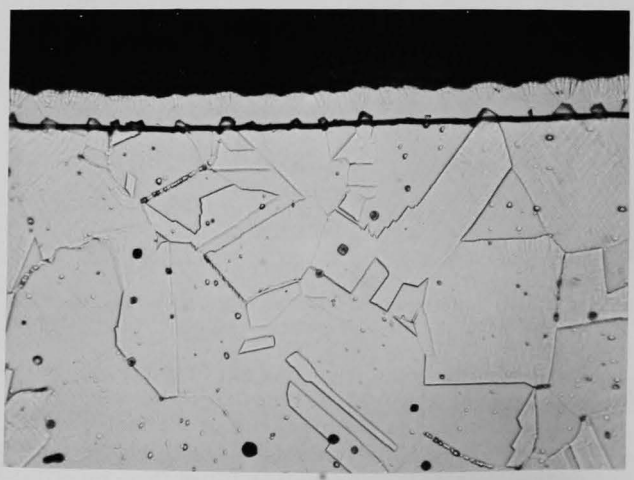

Fig. 4. Section of Type 304 Stainless Steel Tubing, Etched Electrolytically in 10% Oxalic Acid, Taken from 965-1000°F Region of Copper Transfer Loop. Mag. 500X. Neg. No. 47134.

These studies showed that copper does not diffuse in detectable amounts into Type 304 stainless steel under exposure conditions in EBR-II. This is apparently true whether the copper is in solution in the sodium or is deposited into contact with the steel by precipitation from the sodium. In 1969, Atkins[5] reported that there was no penetration of stainless steel by copper dissolved in sodium for much longer exposures at temperatures up to 1300°F.

2. Wear Corrosion of Beryllium-Copper Bushing Rings

Two sets of four narrow bushing rings are used on the lower portion of reactor control-rod subassemblies to minimize wear, reduce leakage of sodium, and prevent galling of stainless steel parts during movement of the subassembly. These rings, which have an L-shaped cross section, were made initially of Berylco 25 (copper containing 2 wt % Be-0.3 wt % Co). Although no difficulty was experienced in operation, surveillance examination of a spent control rod (L-435) after about 10,000 hr in the reactor grid revealed that the exposed surfaces of the Berylco-25 rings were worn or corroded flush with the stainless steel retaining rings. Figure 5 shows the cross section of an exposed Berylco-25 ring.

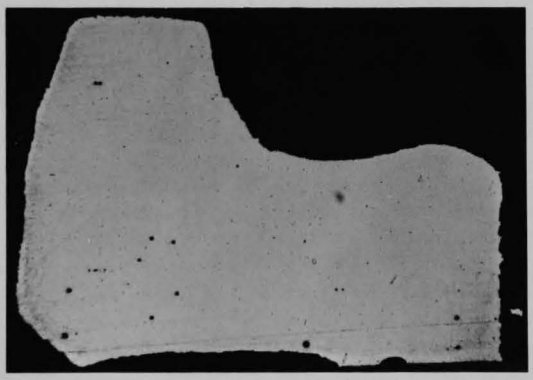

As-polished

Fig. 5. Cross Section of Berylco-25 Bushing from Top Set of Control-rod Subassembly L-435 after 10,000 hr in Reactor Grid. Mag. 40X. Neg. No. 51769.

A test control-rod subassembly (L-457) was prepared. The weights and dimensions of its bushing rings were measured before insertion into the reactor. Rings of an aluminum-bronze alloy--Ampco 18-13 (copper containing 10.6-11.2 wt % Al-3.4-4.0 wt % Fe)--were substituted for half the Berylco-25 bushings in this test subassembly. This control rod was in service in the reactor grid for 5500 hr, of which the reactor was at full power for 1354 hr. The temperature of the sodium at the bushings was approximately 700°F.

As expected, the Berylco-25 alloy rings underwent deleterious changes during irradiation and sodium exposure. The rings lost 14-18% in weight and decreased in diameter by as much as 0.003 in. Their hardness decreased from an initial value of 345 DPH to a final range of 192-204 DPH, and their microstructure showed evidence of the agglomeration of precipitates. Other surveillance samples of Berylco-25 alloys in the reactor showed the same effects, and these are shown in Fig. 6.

Berylco 25 is normally used in a precipitation-hardened condition. The change in microstructure and reduction in hardness noted in this examination indicated that the bushings had been overaged by exposure to the temperature and neutron-flux conditions in EBR-II. Because of vacancy formation, the neutron flux would tend to enhance diffusion in the alloy and thereby would accelerate the overaging process. Because this overaging process causes a loss of hardness and of wear resistance, it may have contributed to the poor corrosion resistance of the rings. Comparison of the loss of metal at two exposure times, shown in Figs. 5 and 7A, indicates that the deterioration progressed as a function of time.

In contrast, the Ampco 18-13 rings lost only about 1% of their original weight, became slightly harder (initial, 147 DPH; final, 168-177 DPH), and showed relatively little change in microstructure. Figure 7 compares an exposed Ampco 18-13 ring with an exposed Berylco-25 ring.

The Ampco 18-13 alloy that is now used for the bushings is relatively unaffected by heat treatment. All phases of the alloy are stable from room temperature to a temperature near the melting point of the alloy. Therefore, heating and cooling of the alloy over a wide range of times and temperatures do not affect its properties. The results of the examination indicate that the properties of this alloy are also stable in the reactor environment. The slight increase in hardness can be attributed to radiation damage rather than to age hardening. Because Ampco 18-13 is not an age-hardening alloy, extended periods of residence in the reactor environment should not cause deterioration of these rings.

3. Bismuth-Tin Incident[6]

The normal tin and bismuth content of reactor-grade sodium is less than 1 ppm. In 1967, the presence of some unexpected radionuclides (^{113}Sn and ^{113m}In) in the primary sodium led to a reexamination of historical sodium analytical samples for tin content. Bismuth was also determined because the logical source of tin contamination was the rotating-seal alloy (Bi-42 wt % Sn). The results of this analytical program indicated that some of the seal alloy had entered the primary sodium in July 1965 and had caused a tin content of 15-20 ppm and a bismuth content of ~25 ppm. The continuous operation of the cold-trap system starting in March 1967 quickly reduced the bismuth to <2 ppm, but it did not alter the tin content. (Tin solubility at the cold trap temperature is >1000 ppm.)

A. Control Specimen before Exposure. Mag. 750X. Neg. No. 51772.

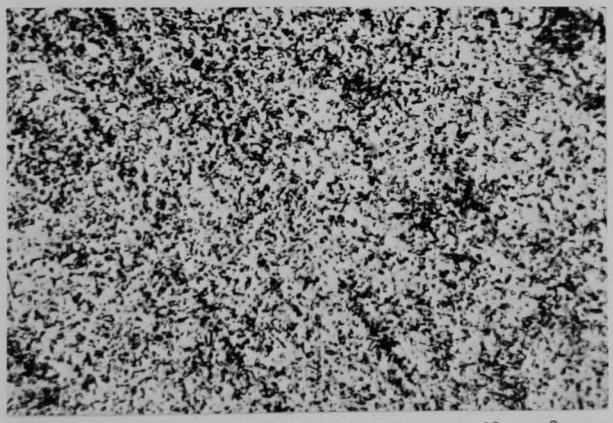

B. Test Specimen after Exposure; Irradiation--1.4 x 10^{19} n/cm^2 (double immersion etch in H_2O_2, NH_4OH, and H_2O, followed by $FeCl_3$, HCl, and H_2O). Mag. 750X. Neg. No. 51773.

Fig. 6. Microstructures of Berylco-25 Alloy before and after Exposure in EBR-II

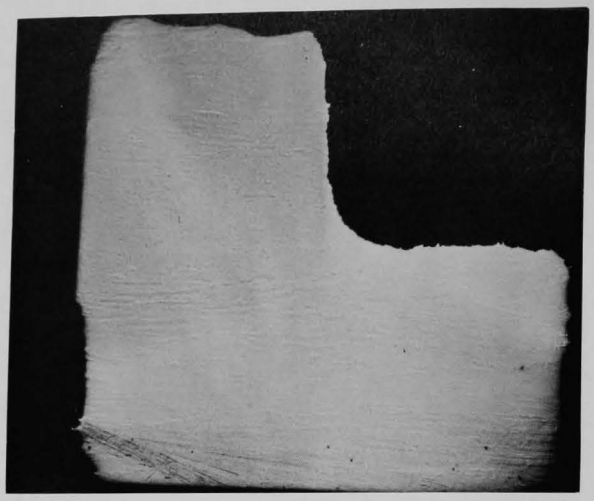

A. As-polished Berylco 25. Mag. 40X. Neg. No. 51770.

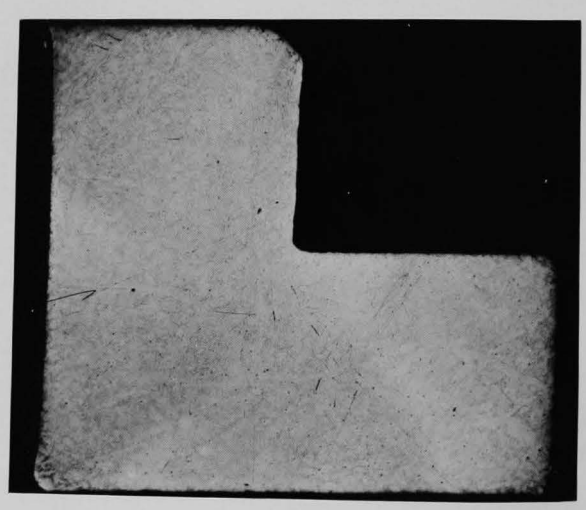

B. As-polished Ampco 18-13. Mag. 40X. Neg. No. 51771.

Fig. 7. Bushing Materials after EBR-II Exposure in Control-rod Subassembly L-457 for ~5500 hr

A portion of a Type 304 stainless steel irradiation capsule that had been exposed for eight months to the primary sodium containing the high tin and bismuth content was sectioned and polished using anhydrous techniques. An electron-beam microprobe examination revealed no tin or bismuth present within the stainless steel or at the surface. This observation, at least as regards tin, tends to be confirmed by the continued presence of tin in the primary sodium at about the initial concentration. Any interaction of the tin with the very large surface area of the stainless steel in the reactor would have depleted the primary sodium.

4. Tantalum Corrosion Product

Tantalum was used to clad the original antimony metal sources used in the reactor. The cladding from source SO-1915 was examined after a total exposure of over five years at 700-725°F.[7] No significant loss of thickness was detected, although surveillance specimens had shown slight weight losses (0.5-3.5 mg/cm^2) caused by interactions with the sodium coolant. The undesirable feature noted with tantalum was the release of a fine-particle, highly radioactive corrosion product into the air of the inspection cell.

B. Failures

Four types of failures have been associated with exposure to EBR-II operating conditions.

1. Apparent Cracking of Type 304L Stainless Steel Fuel-element Cladding

Areas of deep, selective grain-boundary attack were found in the Type 304L stainless steel seamless cladding[8] of fuel element C-249-16 during a metallographic study of fuel-to-cladding compatibility. The element was in the reactor from July 16 to December 4, 1966. Several axial grain-boundary fissures originated in the outer surface of the cladding and penetrated deep into the cladding, as shown in Fig. 8. No similar areas have been found on other fuel elements, although more than 80 polished sections were examined in this investigation.

Two hypotheses of the cause of the attack were offered and evaluated:

a. Slight variations in the normal cleaning or storage of the fuel element could have exposed heat-sensitized stainless steel to concentrated sodium-hydroxide solution.

b. The grain boundaries could have been selectively carburized before or during the exposure to reactor sodium, thereby making the boundaries susceptible to cracking and to attack by etching.

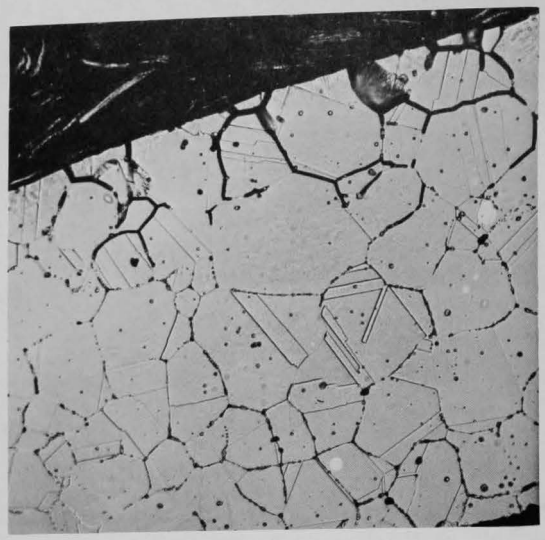

Fig. 8. Cladding of Element C-249-16 after 45-sec Etching in 5% Oxalic Acid. Mag. 400X. Neg. No. 49419.

Sections of seamless and welded Type 304L stainless steel were exposed to 1022°F sodium for up to five weeks in a recirculating system equipped with a cold trap operating at ~215°F. After the specimens were removed from the sodium, they were cleaned by one of two methods:

a. Rinsing with ethanol until the hydrogen-producing reaction had virtually ceased, followed by ultrasonic cleaning in distilled water.

b. Bubbling argon through water at 120°F, and then allowing the moisture-laden argon to impinge on the surface of the specimens. The concentrated solution of sodium hydroxide that formed on the surface of the samples was allowed to remain there for 24 hr. The specimens then were cleaned ultrasonically in distilled water.

Similar specimens were heat-treated in vacuum ampules at 1022°F for five weeks.

Metallographic examination revealed no differences in microstructure between the specimens that underwent the various sodium-removal treatments and the control specimens that were heat-treated in vacuum ampules. Normal variation in the EBR-II cleaning procedure appeared unlikely to have caused the attack observed on element C-249-16. The microstructures that developed when the stainless steel specimens were exposed to clean sodium or to vacuum for up to five weeks were

caused only by the time and temperature of exposure and were independent of exposure to high-temperature sodium and to the subsequent sodium-removal technique.

Bulk chemical analyses of the cladding of element C-249-16 showed an increase in carbon content from an initial value of 0.025 wt % to a final value of 0.035 wt %. Electron-beam microprobe examinations revealed that the carbon concentration was higher in the grain boundaries than in the matrix. A similar examination of another specimen of Type 304 stainless steel exposed in EBR-II showed no detectable carbon increase, even though sensitization had occurred. Thus, it was concluded that the carbon increase in the suspect element was caused by selective carburization at the grain boundaries and not by sensitization.

Various techniques were used to duplicate the microstructure of the cracked element by causing diffusion of carbon into the stainless steel in a sodium environment. The closest duplication of the defected structure was obtained when Apiezon-N grease was used to contaminate the stainless steel surface before sodium exposure. Figure 9 shows these results.

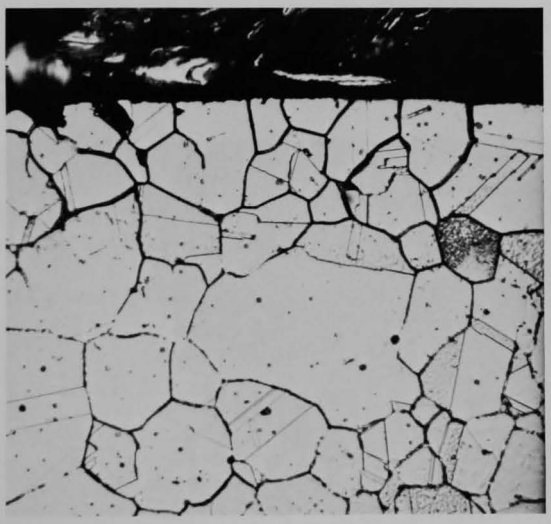

Fig. 9. Type 304L Stainless Steel Tubing That Had Been Streaked with Apiezon-N Grease and Exposed to 1022°F Sodium for One week after a 45-sec Etching in 5% Oxalic Acid. Mag. 400X. Neg. No. 50314.

The isolated occurrence of the attack on C-249-16, its carbon enrichment, and the similarity of its microstructure to that of grease-contaminated stainless steel strongly suggested that carbonaceous contamination during manufacturing or assembly was responsible for the attack.

2. Failure of Type 347 Stainless Steel Valve Bellows

In February 1968, sodium began to leak from a 1/2-in. block valve (designated SN-17) in the EBR-II secondary sodium system. Valve SN-17 had been in service approximately four years and had averaged 24 cycles/yr at an operating temperature of about 580°F. Visual examination of the valve indicated that a Type 347 stainless steel bellows was the source of the leak.

Metallographic specimens were prepared from sections of the bellows containing two previously detected pin holes. Light grinding and polishing revealed the sodium-side entrances to be the two failure locations. A branched crack about 800 μm long and 60 μm wide appeared at the major perforation. The defect responsible for the smaller of the two leaks was about 180 μm long and 10 μm wide.

Transverse sections of the bellows near the defects showed an overlying corrosion product and general intergranular penetration to a depth of 5-10 μm on the sodium side. Figure 10 shows that the penetrations were particularly pronounced in the highly stressed areas of the bellows.

Fig. 10. Transverse Section of Bellows of SN-17 Valve after 10-sec Etching in 5% Oxalic Acid Showing Penetrating Fingers of Sodium Corrosion Product at Highly Stressed Region. Mag. 1000X. Neg. No. 51283.

The general appearance is similar to that obtained when stainless steel is exposed to sodium that contains an oxygen content greater than 100 ppm.[9]

Microlaps were observed in a section of the bellows near the valve handle (cooler end). These probably represent imperfections in the surface of the as-produced bellows and would facilitate the corrosion penetration of the metal.

Chemical analyses performed on well-cleaned sections of the bellows showed that no carburization occurred during service in the reactor.

Several convolutions of the bellows that exhibited intergranular penetration were analyzed using an electron-beam microprobe. An increase in the oxygen concentration, accompanied by a simultaneous decrease in the iron, nickel, and chromium concentrations, was detected in nearly every area of penetration. There was no evidence of a carbon-concentration gradient from the matrix to the areas of intergranular penetration. Such evidence substantiated the metallographic observation that the corrosion product appeared to be an oxide.

The probable explanation for the intergranular penetration and failure was found when it was learned that valve SN-17 might have been used in an oxygen-contaminated sodium system before it was installed in EBR-II. The valve had been acquired on an emergency basis from another Argonne division.

Cleaning a bellows-seal valve for reuse is difficult, even when the bellows surface is absolutely smooth, because any sodium hydroxide retained after washing can cause caustic cracking after the application of heat and stress. In the case of the SN-17 valve, microlaps in the bellows surface and deep intergranular penetrations (from its earlier service) would have made it virtually impossible to remove adequately all traces of sodium hydroxide.

3. Failure of Inconel-600 Rupture Disc

In March 1969, failure of an Inconel-600 rupture disc from the EBR-II secondary sodium system was detected. The disc (12-in. dia x 0.003 in. thick) was exposed to 775°F sodium on one side and to air on the other.

Visual examination revealed that the disc was perforated about 3/4 in. from a circumferential restraining ring and left a network of thinned metal and open areas about 1/2 in. in diameter. When the disc was initially removed from the system, the perforated area was covered with a hard, crusted corrosion product that had restricted the flow of sodium. Qualitative analysis of the corrosion product revealed no elements extraneous to Inconel 600.

Figure 11 shows that microscopic examination of an as-polished transverse section of the corroded network indicated extensive intergranular penetration, cracking, and loss of whole grains in most areas. In other locations, the metal was smoothly corroded with little or no indication of intergranular penetration. The original perforation could not be located precisely within the network area. A greater portion of the attack on the metal occurred from the air side of the rupture disc.

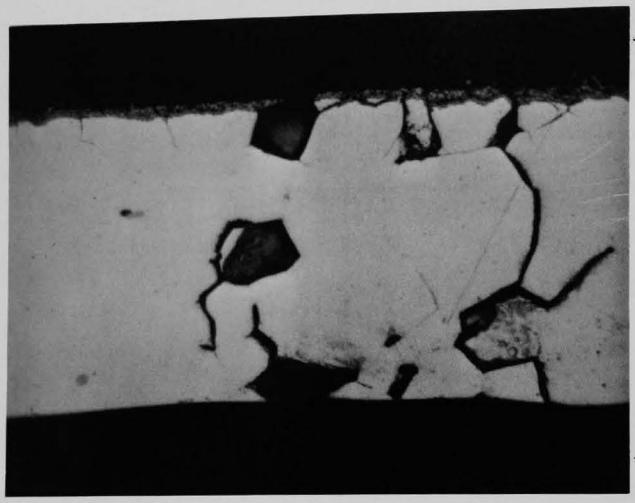

Fig. 11. As-polished Transverse Section of the Corroded Network Showing Cracks and Missing Grains Adjacent to Perforated Area in Inconel-600 Rupture Disc. Mag. 800X. Neg. No. 51087.

An electron-beam microprobe analysis of the metal in the perforated area indicated a significant increase in the carbon content of the grain boundaries as compared with the levels detected in uncorroded areas of the disc. These findings substantiated suspicions that the Inconel 600 may have suffered embrittlement as a result of contamination by some carbonaceous material (grease, thread lubricant, etc.) during manufacturing or assembly. The microprobe results showed that the layer on the air side of the disc was enriched in nickel with respect to the composition of the alloy matrix.

Apparently, the initial perforation or crack permitted sodium to react with the atmosphere on the outside of the disc and then to form sodium oxide and sodium hydroxide. As these compounds combined with the metallic sodium present and reacted with the disc metal, they caused cracking around the original penetration site. The caustic stress-corrosion cracking of Inconel 600 is well established for concentrated caustic solutions at elevated temperatures.[10]

4. Fracture of Type 420 Stainless Steel Roll Pin

A Type 420 stainless steel roll pin in a sensing rod fractured in service after approximately six years' exposure to 700°F primary-tank sodium. This pin and three similar pins from a second sensing rod were examined metallographically. The dimensions of the pins were 5/32 in. OD x 0.09 in. ID x 1 in. long. The pins were hollow, with a closed "c" cross section. Their function was to secure a solid shaft within a larger hollow concentric shaft at three places along the sensing rod, which was used to locate subassemblies in the storage basket.

All pins exhibited surface scales, which appeared to be oxides. The reaction layer was more evident on the inner surface than on the outer one. The thickness of the reaction layer on the failed pin was approximately 2×10^{-4} in. at its maximum; however, as shown in Fig. 12, the attack was not uniform. The product penetrated intergranularly (also shown in Fig. 12) to depths of about 5×10^{-4} in. The same type of surface attack, although developed to a lesser extent, was found on an unexposed pin, suggesting that the forming and heat-treating operations before use were largely responsible for the type of reaction layer.

As-polished

Fig. 12. Inner Surface of Failed Roll Pin Examined at Idaho. Mag. 1000X. Neg. No. 10B1-6.

The microstructure of all pins was that of partially tempered martensite, as shown in Fig. 13; immersion in nital etchant (glyceregia)* revealed a slightly decarburized zone, about 4×10^{-4} in. deep, on the pin exposed to primary sodium. Bulk chemical analyses gave values of

*Glyceregia: a mixture by volume of 1 part conc HNO_3, 2 parts conc HCl, and 3 parts glycerin.

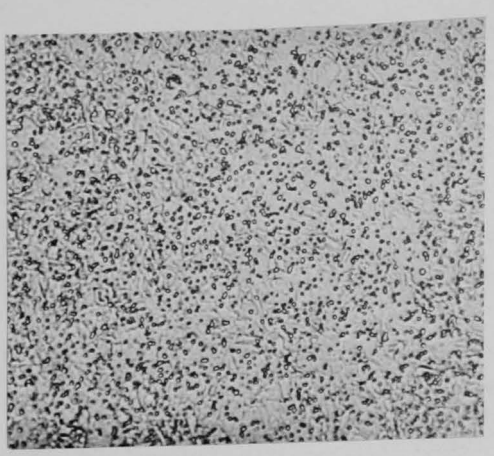

Fig. 13. Typical Microstructure of Type-420 Stainless Steel Roll Pins after 10-sec Etching in Glyceregia. Mag. 1000X. Neg. No. 50776.

0.35 ± 0.01 wt % carbon for the pins; this figure was well above the 0.15 wt % carbon specification for Type 420 stainless steel.

Microhardness traverses failed to reveal any significant hardness gradients. The values ranged from 417 to 468 DPH. The converted values of 397-433 BHN are somewhat less than the typical values of 461-534 BHN reported[11] for quenched and stress-relieved Type 420 stainless steel.

Because the examination revealed nothing to pinpoint the cause of failure, the low impact strength of Type 420 stainless steel, coupled with the micronotches noted on the surface, probably resulted in fracture during the relatively minor shock loading encountered in use.[12] There are now no similar pins in operating components of the EBR-II.

C. Examination of Components

A wide variety of components were examined in this study, and several are discussed here.

1. Type 304L Stainless Steel Fuel Cladding

Numerous samples of fuel-element cladding have been examined by optical microscopy to determine the effects of the reactor primary sodium and the sodium-removal operation on the Type 304L stainless steel cladding. The outer surface of each element is subjected to flowing sodium at 700-1100°F. The inner surface of the cladding is exposed to stagnant sodium that fills the annulus between the cladding and the fissium-alloy* fuel pin.

Samples have been taken from elements subjected to a wide variety of fluences, operating temperatures, lengths of exposure to the primary sodium, and postirradiation handling and storage procedures. A brief history of some of the elements from subassemblies that were subjected to unusual conditions and then subsequently examined is listed below.

*Composition: 2.27-2.61 Mo, 1.78-2.10 Ru, 0.23-0.33 Rh, 0.15-0.23 Pd, 0.07-0.13 Zr, 0.028-0.052 Si, 0.004-0.016 Nb, balance uranium.

C-2186S. This subassembly was irradiated to 1.4×10^{22} n/cm^2; however, the sodium flow through the subassembly was restricted to simulate fuel and cladding temperatures similar to those expected at 62.5-MW operation.

C-2169. This subassembly was irradiated to 2.3×10^{22} n/cm^2 (the highest to date for driver fuel) at approximately 950°F maximum cladding temperature and then subjected to the normal sodium-removal process.

C-2193S. This subassembly was irradiated to 1.1×10^{22} n/cm^2, subjected to the sodium-removal operation, and disassembled, and nondestructive examination was performed on the elements. The subassembly then was rebuilt, irradiated an additional 0.3×10^{22} n/cm^2 to a total of 1.4×10^{22} n/cm^2, and subjected to another sodium-removal operation. This subassembly contained 70% enriched fuel and therefore operated at temperatures similar to those expected at 62.5-MW operation (maximum cladding temperature 1040°F).

C-278. This subassembly was irradiated to a maximum fluence of 1.5×10^{22} n/cm^2 and then cycled between the reactor and the FCF air cell four times. During each cycle, this subassembly was exposed to the primary sodium for 24 hr and then subjected to the sodium-removal operation.

B-339. This subassembly was irradiated to 1.1×10^{22} n/cm^2 and subjected to the normal sodium-removal operation. Several elements from the subassembly were stored in a canal at the Idaho Nuclear Chemical Processing Plant for 24 months.[13]

Examination of the cladding from these and other EBR-II driver-fuel elements has shown no evidence of selective attack by the sodium environment. The only microstructural change that occurs is sensitization (precipitation of carbides at the grain boundaries). For operation at higher temperatures (i.e., 1080°F maximum), the degree of sensitization of the cladding has been observed to be most severe in the region just above the reactor midplane and least severe (or nonexistent) at the bottom of the fuel element (as shown in Fig. 14).

Carbide precipitation, as shown in Fig. 15, has been frequently observed in the grain boundaries and has been more severe near the inner and outer surfaces of the cladding. Because the degree of sensitization has been similar at the two surfaces, the reactor primary sodium has been neither carburizing nor decarburizing the cladding to any significant extent. The degree of sensitization has not always been uniform in a sample but has varied randomly at various positions around the circumference of the samples.

96B3-4 Top 300X

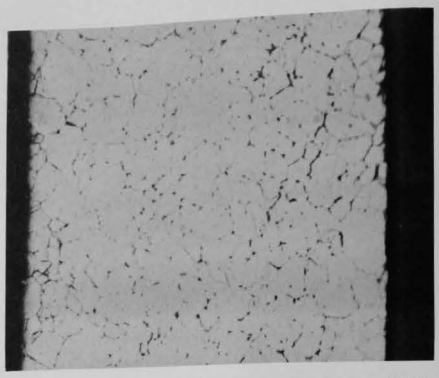

96B3-1 Top 300X

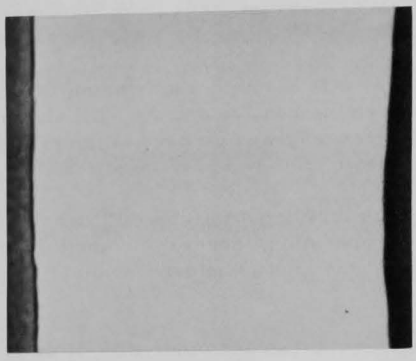

96B2-4 Midlength 300X

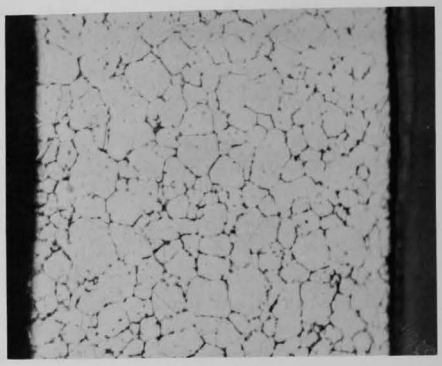

96B2-1 Midlength 300X

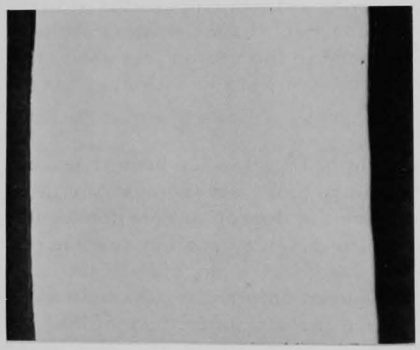

96B1-4 Bottom 300X

(As-polished)

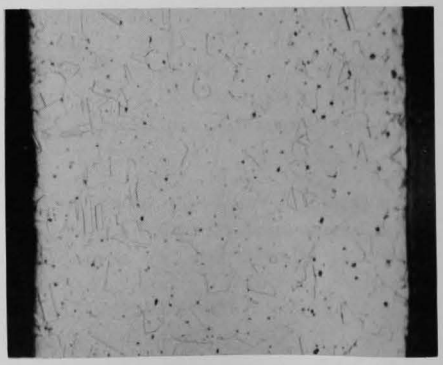

96B1-1 Bottom 300X

(Oxalic acid electroetch)

Fig. 14. Irradiated Cladding Microstructure of Element 63--Subassembly C-2186S as a Function of Position

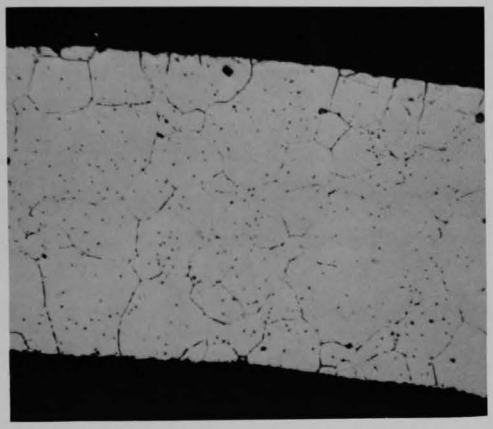

141A3-3 Midlength 250X

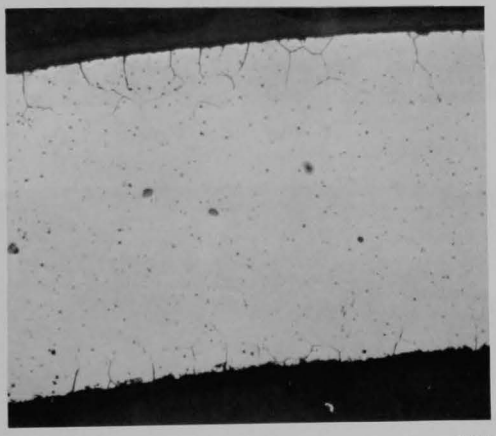

141A4-3 Top 250X

Fig. 15. Transverse Sections of Irradiated Cladding from Element 41--Subassembly C-278 after Etching in 10% Oxalic Acid Showing Sensitization at Both Surfaces

Examination of as-received samples of the cladding tubing after they were heat-treated in a vacuum for varying periods of time at 1100°F has revealed sensitized microstructures similar to those observed in the irradiated cladding (see Fig. 16). Chemical analysis of 0.002-in.-thick layers machined from the surface of as-received tubing has shown twice the carbon concentration near the surface than at the center of the tubing wall. This variation of carbon concentration in the tubing has appeared to occur during the fabrication of the tubing by the manufacturer and accounts for the effect noted in Fig. 15.

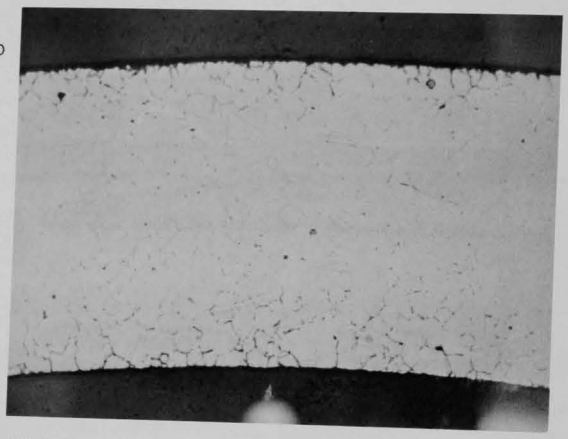

158A3-1 A. After 1-hr exposure 250X

114B2-1 B. After 8-hr exposure 250X

Fig. 16. Microstructures of As-received Cladding after Vacuum Heat Treatment at 1100°F and Etching in 10% Oxalic Acid

The effect (or lack of it) of the sodium-removal process on the irradiated cladding has also been investigated. Examination of cladding samples that have been subjected to multiple sodium-removal operations or have been stored under water have shown the same microstructures and lack of corrosive attack as those receiving a single sodium-removal operation and short storage periods in air prior to examination (see Fig. 17).

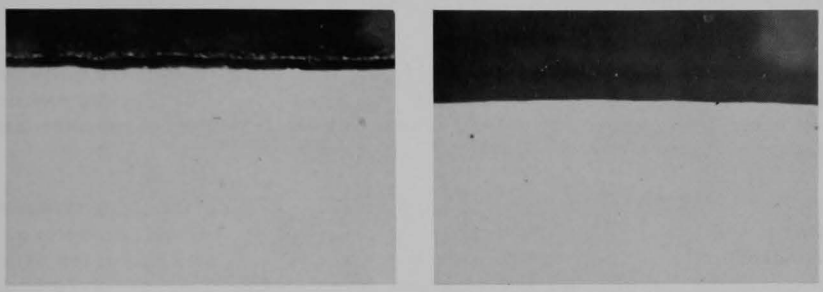

110B1-1 Bottom 400X 110B4-1 Top 400X

As-polished Samples from Element 22, Subassembly B-339 (stored in canal)

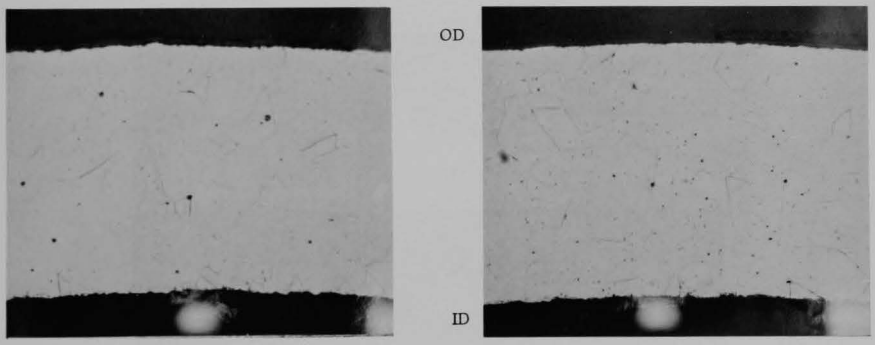

141A3-2 Midlength 200X 141A4-2 Top 200X

Samples Etched with 60 cc Lactic Acid, 30 cc HNO_3, 10 cc HCl, and 0.5 g $FeCl_3$ from Element 41, Subassembly C-278 (multiple sodium removal)

Fig. 17. Lack of Corrosive Effect of Sodium-removal Treatment or Storage on Irradiated Cladding

2. Type 304 Stainless Steel Guide Thimbles

Replaceable tubes of hexagonal cross section are used to guide control and safety rods in their movement through the core of the EBR-II. One of these tubes has been examined in detail.[14] Only those aspects of the examinations that relate to coolant interactions will be discussed here.

The guide thimble for control rod number 12 was removed after 15,500 MWd in the reactor. Sections were taken at two points which had seen different temperatures and total fluences. The section exposed at a sodium temperature of ~806°F and a fluence of 4.6×10^{22} n/cm^2 revealed a solution-annealed microstructure similar to that of the as-received tube. Another section, exposed at a slightly higher temperature and a lower fluence (~860°F, 1.2×10^{22} n/cm^2), exhibited some carbide precipitation at the grain boundaries.

The sodium-exposed surfaces of both sections were quite uniform with numerous shallow, smooth-bottomed pits. Microprobe examination showed no change in surface concentrations for iron, chromium, and nickel.

A similar guide tube for a safety-rod assembly was removed after a somewhat longer exposure (~$4\frac{1}{2}$ years of operation). As before, representative sections were taken with several different histories of temperature and total fluence as shown in Table III. Figures 18-20 illustrate the corrosion interface for the different exposure conditions.

TABLE III. Specimens from Safety-rod Guide Thimble[a]

Designation	Estimated Temp, °F	Estimated Total Fluence, n/cm^2
H14	700	2×10^{22}
H12	720	6×10^{22}
H7	806	2×10^{22}

[a]Original guide thimble in reactor position 3D1.

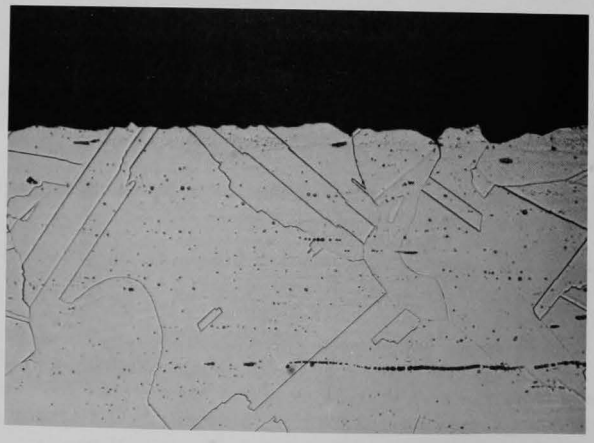

Fig. 18. Corrosion Interface for Specimen H14 after 15-sec Etching in 5% Oxalic Acid. Mag. 250X. Neg. No. 52076.

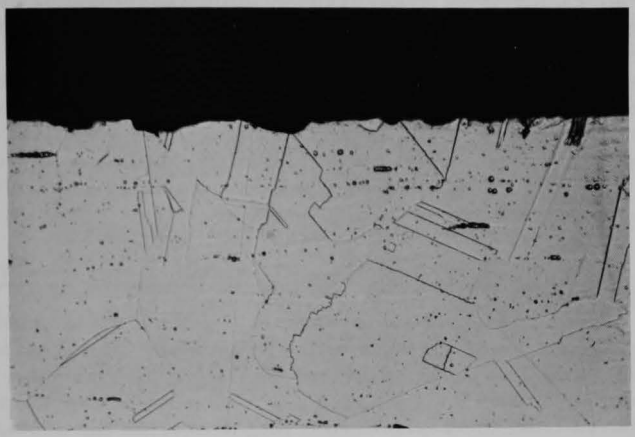

Fig. 19. Corrosion Interface for Specimen H12 after 15-sec Etching in 5% Oxalic Acid. Mag. 250X. Neg. No. 52077.

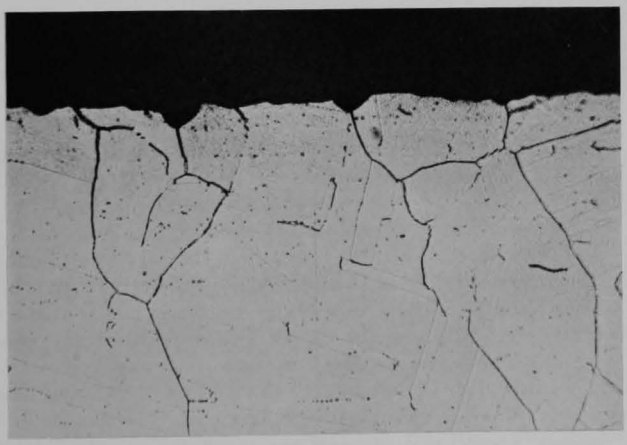

Fig. 20. Corrosion Interface for Specimen H7 after 15-sec Etching in 5% Oxalic Acid. Mag. 250X. Neg. No. 52075.

The two samples exposed at the lower temperature showed less surface erosion than did H7, but no meaningful difference in total thickness was found among the three specimens. (No measurements had been taken of the unirradiated thickness.) The point of emergence of a grain boundary onto the exposed surface was a favored site for dissolution, but penetrations did not appear to extend appreciably into the metal, and no grain boundaries were visible in the as-polished conditions. A microprobe analysis of specimen H7 in which no compositional variations in iron, nickel, or chromium were detected near the surface or in the vicinity of the grain boundaries supported the visual observations. There was no detectable carbon concentration in the grain boundaries.

3. Gripper Assembly from Control-rod Driver Number 6

The control-rod subassemblies are attached to and disconnected from their respective drives by a gripper assembly. Because of a failure of a bellows in the gas phase of the reactor, a gripper assembly became available for examination. The drive was cut up for easier disposal after it was removed from the reactor; so trying to analyze the probable cause of the bellows failure was not profitable. However, the gripper components offered a good opportunity to evaluate the extent of carbon mass transport occurring in EBR-II.

Drive No. 6 was installed in the original loading of the reactor and removed in January 1968. The gripper end was in the outlet sodium plenum and was exposed to 830-840°F sodium at a reactor power level of 45 MW. During shutdown, the temperature would normally have been 700°F.

a. Clamp Gripper. The sections of the clamp gripper chosen included a semicircular (3/8-in. dia) wear piece of Stellite (No. 3 or 6) welded to Type 304 stainless steel.

The Stellite surface was regular and smooth, as shown in Fig. 21, and the microstructure at the surface showed no deviation from that of the bulk material. The weld bridge between the Stellite and the Type 304 had a crack. Etching the crack area revealed that the crack was not at the junction of the two different metals, but was a crack in the Stellite 6B weld material. Because cracks of this type have been noted in several other instances, a change in welding practice has been initiated. Currently, Type 308 weld rod is used successfully to join Stellite and Type 304 stainless steel.

b. Tip Sensor. A section of Type 420 stainless steel (12 to 14 wt % chromium) was examined. The surface was smooth with essentially no adherent corrosion product. Electroetching revealed an essentially continuous microstructure to the very edge and no evidence of significant carbon migration.

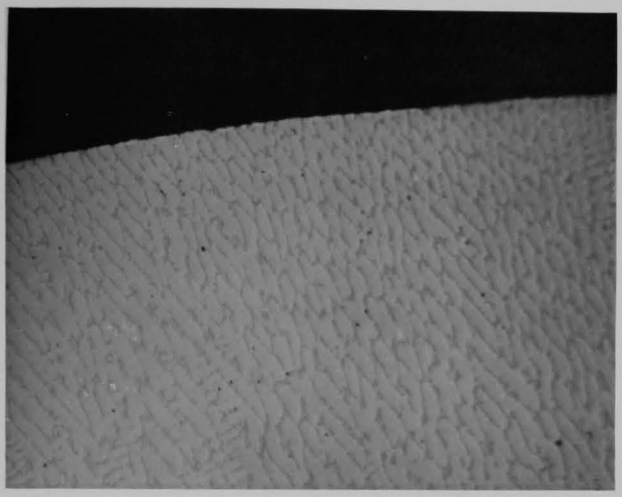

Fig. 21. As-polished Stellite Clamp Gripper. Mag. 250X. Neg. No. BK3216.

c. Jaw Gripper. The jaw gripper, fabricated of chromium-plated Type 420 stainless steel, allowed a determination of the durability of chromium plate exposed to EBR-II sodium. As shown in Fig. 22, slightly less than 0.003 in. of plating (initially specified as 0.0005-0.0035 in.) was present on the outer surface of the part. The plating was fissured, but this

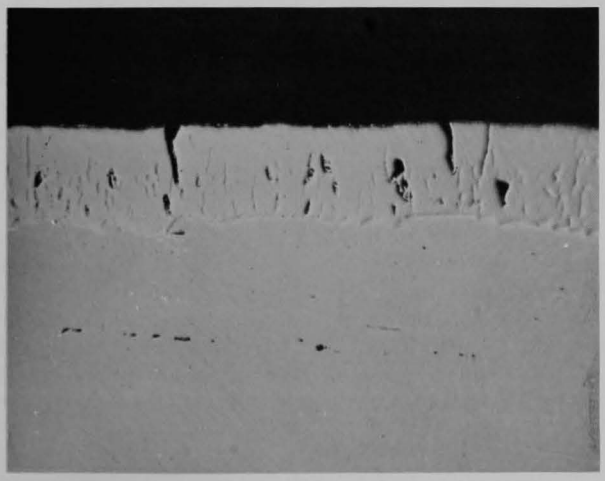

Fig. 22. As-polished Outer Surface of Jaw Gripper Showing Thick Chromium Plating. Mag. 250X. Neg. No. BK3215.

is a characteristic of thick chromium plating and probably was not a result of sodium exposure. Much less chromium was present on the inner surface of the jaw; in one place on an inner radius, the chromium was missing completely. As shown in Fig. 23, this unplated area appears to have suffered slight decarburization to a depth of <0.001 in.

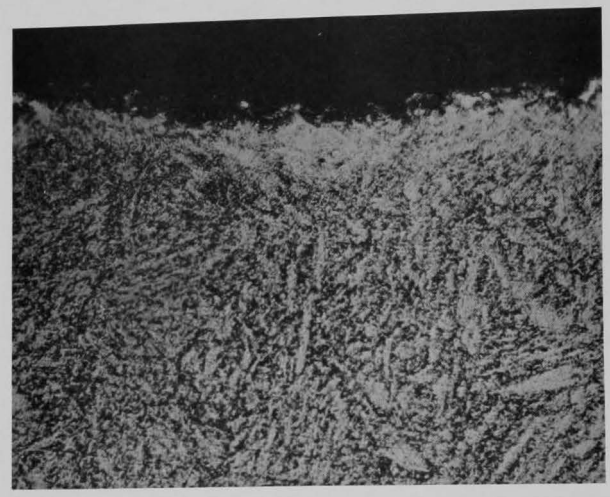

Fig. 23. Compositional Zone at Unplated Surface of Jaw Gripper after 10-sec Etching in Warm 10% Nital. Mag. 500X. Neg. No. BK3225.

d. Pin. The pin was made of Rex AA tool steel. No evidence of a decarburized zone was detected on either a chromium-plated area or an exposed bare end. There were several small irregular-shaped pits on the exposed end that could have been the result of sodium attack, but more likely they were the result of the mechanical efforts to remove the pin.

4. Type 304 Stainless Steel Piping (Secondary Sodium System)

A section of Type 304 stainless steel pipe (2 in. nominal) was removed from the reactor's secondary-sodium system vent line (designated as 2-31-549) during the major shutdown of EBR-II in the winter of 1968-69. The specimen was cut about 18 in. from the main (12 in.) sodium supply line leading to the steam generating plant (designated 2-31-500). The primary objective of the examination was to determine whether a significant amount of carbon migration had occurred from the Croloy-$2\frac{1}{4}$ alloy steam generator of the secondary system to the austenitic stainless steel piping.

The 2-in. pipe had been in operation for approximately six years at a sodium flowrate of 3-5 gpm. The sodium temperature was about 830°F when the reactor was producing heat; during shutdown, the temperature

dropped to about 580°F. The section that was chosen did not represent the optimum specimen for study, because greater mass transfer of carbon might be expected to occur in the Type 304 intermediate heat exchanger (or even in the Type 304 stainless steel piping immediately downstream from the Croloy-$2\frac{1}{4}$ steam generators), but no feasible way of obtaining these other specimens could be devised.

Sodium in contact with the pipe had a typical analysis of less than 10 ppm oxygen (by the mercury-amalgamation method) and about 2 ppm carbon (by the oxyacidic-flux method).

The exterior (air side) of the pipe had a thin oxide film, as is normal for Type 304 stainless steel heated in the operating temperature range. The interior wall surface looked metallic, but was somewhat frosted or etched. Metallographic study of a transverse section of the pipe corroborated the appearance of slight attack on the inner surface, as is seen in Fig. 24; the air-exposed outer surface was smooth and unattacked, as shown in Fig. 25. Close examination of the inner surface at higher magnification (see Fig. 26) showed a gray coating varying in thickness from 3 to 6 μm on the metal. Although the coating appeared to be a deposited metal powder rather than a corrosion product, no positive identification was made. The coating was brushed off and dissolved in 6N HCl, and the solution was analyzed spectrographically. The major constituents were iron, chromium, and nickel in the ratio of 20:4:1. The accuracy of the analysis was not adequate to decide if this was a meaningful deviation from the 9:2:1 ratio in Type 304 stainless steel.

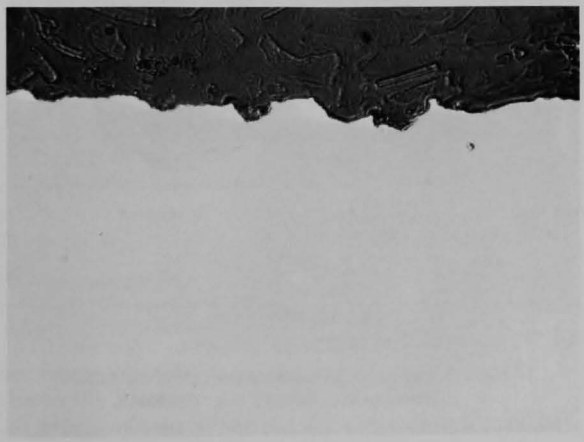

Fig. 24. As-polished Inner (Sodium) Surface of Secondary System Pipe. Mag. 400X. Neg. No. 51412.

Fig. 25. As-polished Outer (Air) Surface of Secondary System Pipe. Mag. 400X. Neg. No. 51411.

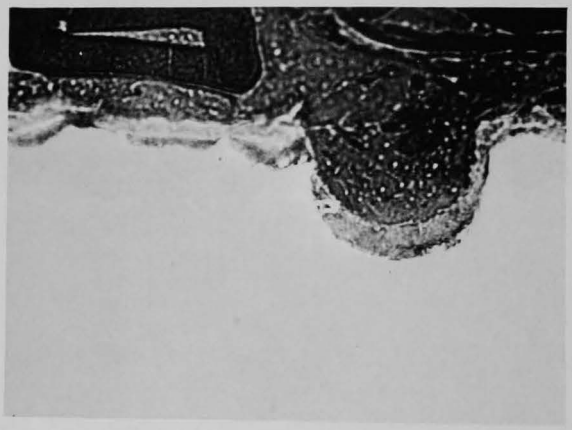

Fig. 26. Deposit on As-polished Inner (Sodium) Surface of Pipe. Mag. 1000X. Neg. No. 50413.

Some of the grain boundaries near the inner (sodium) surface were selectively attacked to a depth of 2-3 mils during electrolytic etching in 5 wt % oxalic acid, as shown in Fig. 27. This attack is usually a result of the movement of carbon (or nitrogen) into the boundaries during the high-temperature exposure. The inner surface of the pipe was removed to a maximum depth of 3 mils, and the chips were analyzed chemically for carbon and nitrogen. For comparison, chips taken from the center of the pipe wall were also analyzed. The results are shown in Table IV.

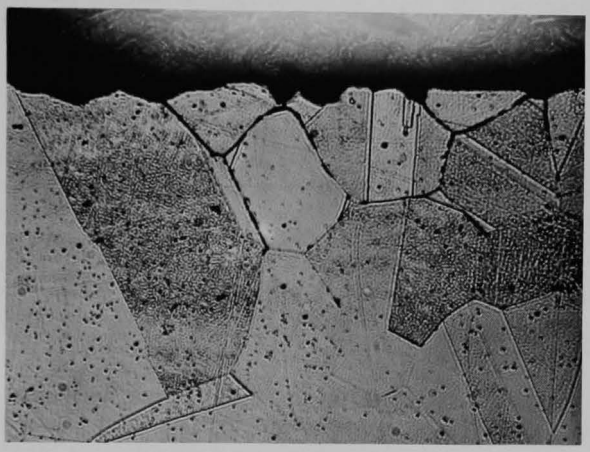

Fig. 27. Inner (Sodium) Surface after Electrolytic Etching by 5% Oxalic Acid for 45 sec. Mag. 400X. Neg. No. 50414.

TABLE IV. Chemical Analyses of Type 304 Stainless Steel Pipe after Sodium Exposure

Location	Carbon, wt %	Nitrogen, wt %
Near sodium surface (0.003-in. cut)	0.13	0.022
Center of pipe wall	0.06	0.021

Although the carbon content of the surface metal layer exposed to the sodium environment increased significantly, the increase may not have been due to the transfer of carbon from the sodium to the pipe wall. No unexposed piece of pipe from the same heat was available for comparison to verify this carbon transfer.

The presence of carbon in the grain boundaries at the surface, coupled with the shallow pitting observed, raised the possibility of crack

initiation during plastic deformation. A section of pipe was flattened and reexamined. No crack initiation was noted under the high-power microscope, either as-polished or after electrolytic etching. The structure was identical to that of the as-exposed piece of pipe.

D. Evaluations of In-reactor Corrosion

Final judgment as to the adequacy of a component for service in the LMFBR primary system must be based upon actual performance of the component. If the component involves new materials, a necessary intermediate step is the in-reactor testing of such materials.

1. Spool Specimens

Vanadium-titanium and vanadium-titanium-chromium alloys had demonstrated sufficient corrosion resistance in low-oxygen sodium at temperatures up to 1300°F[15,16] to warrant consideration as alternates to stainless steel for LMFBR fuel jacketing. Accordingly, a series of exposures of these alloys was carried out in the primary sodium of EBR-II. Type 304 stainless steel was included to serve as a standard of comparison. In addition, a variety of high-temperature, high-strength alloys of potential LMFBR interest were also included.

The samples were cylindrical spools 9.5 mm OD x 4.2 mm ID x 19.2 mm long (5.73 cm^2 exposed surface area) mounted on Type 304 stainless steel rod extensions* of fuel-element test capsules located in the core of EBR-II. The exposure positions used were about 28 in. above the core center: position 4N2 for all but subassembly X011; position 2N1 for subassembly X011. The samples were on the downstream end of the test assembly and thus were exposed to flowing sodium at the exit temperature of the given element.

The method of assembly is illustrated in Fig. 28, which shows the three capsules included in subassembly X009 after removal (and initial cleanup) from the reactor.

The results of the first experiment have been reported,[17] but are repeated here for completeness and because improved methods of calculation have resulted in presumably more accurate values of fluence, temperature, and sodium velocity.

The composition and metallurgical conditions of the samples are listed in Tables V and VI. The vanadium and vanadium-base alloys were furnished by the Foundry and Fabrication Technology Group of the ANL Materials Science Division. The other alloys were obtained from commercial sources.

*Inconel 600 or X-750 springs were used to prevent axial sample movement.

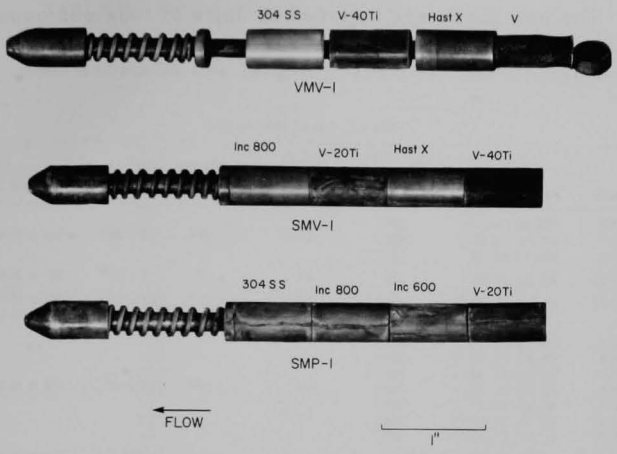

Fig. 28. EBR-II Corrosion Samples. ANL Neg. No. 106-9287.

TABLE V. Composition of Vanadium-base Alloys

Alloy	Heat Treatment and Code[a]	Alloying Elements,[b] wt %		Impurities,[b] ppm			
		Ti	Cr	C	O	N	H
Unalloyed vanadium	Annealed 1740°F; D	-	-	420	390	250	50
V-20 wt % Ti	Stress relieved 1290°F; E	20.2	-	480	358	138	13
V-20 wt % Ti	Annealed 1650°F; H	20.2	-	480	358	138	13
V-40 wt % Ti	Annealed 1650°F; T	41.0	-	240	790	260	99
V-15 wt % Ti-7.5 wt % Cr	Annealed 1650°F; W	7.5	14.9	250	702	400	16

[a]Code designation will be used in Table VII to facilitate communication.
[b]Billet analysis.

TABLE VI. Composition of High-temperature Alloys

Alloy and Code	Alloying Element, wt %						
	Fe	Cr	Ni	Mo	Co	C	Others
304 SS; annealed; A	Balance	19.20	9.56		0.18	0.08	Mn 0.92; P 0.017; S 0.014; Si 0.66
316 SS; cold-drawn; Y	Balance	17.01	12.87[a]	2.30		0.05	Mn 1.62; Si 0.68; P 0.036; S 0.028; Cu 0.18
Hastelloy-X; solution-treated; K	18.69	22.07	Balance	8.99	1.31	0.13	W 0.81; Si 0.90; Mn 0.66; P 0.008; S 0.008
Incoloy 800; annealed; M	46.32	20.38	30.83[a]			0.08	Mn 0.95; S 0.007; Si 0.37; Cu 0.30; Al 0.39; Ti 0.35
Inconel 600; annealed; S	6.75	15.64	77.01[a]			0.05	Mn 0.18; S 0.007; Si 0.27; Cu 0.07
Timken 16-15-6;[b] annealed; P	Balance	15.0/17.5	14.0/17.0[a]	5.5/7.0		0.08 max	Mn 6.5/8.5; Si 1.00 max; N 0.15/0.25
Timken 16-25-6;[b] annealed; V	Balance	15.0/17.5	24.0/27.0[a]	5.5/7.0		0.12 max	Mn 2.00 max; Si 1.00 max; N 0.10/0.20
Multimet; annealed; X	Balance	21.59	20.22	2.94	20.39	0.12	W 2.50; Si 0.69; Mn 1.47; N 0.12; Nb+Ta 1.13; P 0.016; S 0.015

[a]Includes small amount of cobalt.
[b]Specification.

The samples were exposed in units of four per capsule. The number of capsules per subassembly varied from one to seven. Table VII lists the subassemblies, capsules, sample, and exposure data.

TABLE VII. Sodium-exposure Data

Subassembly	Capsule	Sample Numbers[a]	Sodium Temp at Top of Capsule,[b] °F	Sodium Velocity, m/sec	Fluence, n/cm^2 Total	Fluence, n/cm^2 >0.1 MeV	Equivalent Full-power Days	Total Time in Primary Tank, months
X009	SMP-1 SMV-1 VMV-1	A04; M6; S3; H1 M7; H5; K1; T1 A07; T3; K8; D6	849 820 887	4.1[c]	7.2×10^{20}	2.1×10^{20}	119 at 45 MW	9
XG05	NMV-11	A8; S0; K4; M4	820	4.1	1.7×10^{21}	5×10^{20}	281 at 45 MW	31
XA08	NMV-12	A4; S8; K7; M9	844	4.0	2.5×10^{21}	7.3×10^{20}	278 at 45 MW 136 at 50 MW	43
X011	SOV-3 HOV-4 TVOV-1 SOV-7 SOV-1 HOV-10 HOV-15	W2; P3; H4; S2 H3; M0; P5; D2 X2; M5; Y4; P4 T2; V3; W3; K2 A0; W1; V4; K3 V1; X1; E6; K5 K0; H2; S1; A9	838 826 843 847 819 848 833	4.8	7.8×10^{20}	2.3×10^{20}	128 at 45 MW	15
X015	TVMV-1 NMP-1	A1; S4; K6; M1 A2; E1; H6; E2	851 873	4.0	1.5×10^{21}	4.2×10^{20}	160 at 45 MW 82 at 50 MW	29

[a]Samples listed in order from top. Letters define material according to codes in Tables V and VI. Numbers are sample numbers within a materials group and are for identification purposes only.
[b]Calculated by W. J. Larson using the HECTIC code, which takes into account radial heat transfer between coolant channels within the subassembly. Original values reported for X009 were calculated using measured inlet temperatures and fission rates. The present values are presumably more accurate.
[c]Originally reported as 3.7 m/sec.

Oxygen concentration of the sodium during the first portion of these exposures is known within only a relatively narrow range (i.e., probably between ~2 and 8 ppm). This is unfortunate, because oxygen concentration is the most important factor controlling the behavior of vanadium alloys in sodium at the temperatures encountered in this program.

Weight-change data were determined for all materials and are listed in Tables VIII and IX for the vanadium alloys and high-temperature

TABLE VIII. Weight-change Data for Vanadium Alloys[a]

Material	Days at Power	Capsule No.	Temp, °F	Weight Loss, mg/cm^2
V	119	VMV-1	887	620[b]
	128	HOV-4	826	303[b]
V-20 wt % Ti	119	SMV-1	820	5.9[c]
	119	SMP-1	849	12.2[c]
	128	HOV-4	826	8.8
	128	SOV-3	838	12.5
	128	HOV-15	833	10.7
	128	HOV-10	848	13.5
	242	NMP-1	873	27.0
	242	NMP-1	873	31.8
	242	NMP-1	873	30.2
V-40 wt % Ti	119	SMV-1	820	3.7[c]
	119	VMV-1	887	10.4[c]
	128	SOV-7	847	6.1
V-15 wt % Ti-7.5 wt % Cr	128	SOV-7	847	7.4
	128	SOV-1	819	7.6[c]
	128	SOV-3	838	7.3

[a]Temperatures of exposure and days at full power are included in this table. For other exposure information, see Table III.
[b]Because so much of the sample disappeared, this number is of no quantitative significance.
[c]No surface-hardened layer was detected on these specimens.

TABLE IX. Weight-change Data for High-temperature Alloys

Material	Days at Power	Capsule No.	Calculated Temp, °F	Weight Change, mg/cm^2
304 SS	119	SMP-1	849	a
	119	VMV-1	887	a
	128	SOV-1	819	-0.53
	242	NMP-1	873	-6.3
	242	TVMV-1	851	-15.1
	281	NMV-11	820	+0.21
	414	NMV-12	844	-0.12
316 SS	128	TVOV-1	843	-0.09
Hastelloy-X	119	SMV-1	820	a
	119	VMV-1	887	a
	128	SOV-1	819	+0.05
	128	HOV-15	833	0.0
	128	SOV-7	847	-0.12
	128	HOV-10	848	+0.33
	242	TVMV-1	851	-3.0
	281	NMV-11	820	+0.08
	414	NMV-12	844	+0.05
Incoloy 800	119	SMP-1	849	a
	119	SMV-1	820	a
	128	HOV-4	826	a
	128	TVOV-1	843	0.0
	242	TVMV-1	851	-1.8
	281	NMV-11	820	-0.07
	414	NMV-12	844	-0.11
Inconel 600	119	SMP-1	849	a
	128	SOV-3	838	0.0
	128	HOV-15	833	+0.12
	242	TVMV-1	851	-9.7
	281	NMV-11	820	+0.09
	414	NMV-12	844	0.0
Timken 16-15-6	128	SOV-3	838	0.0
	128	HOV-4	826	a
	128	TVOV-1	843	-0.07
Timken 16-25-6	128	SOV-7	847	0.0
	128	HOV-10	848	a
	128	SOV-1	819	+0.09
Multimet	128	TVOV-1	843	0.0
	128	HOV-10	848	+0.26

[a]No data available.

alloys, respectively, in order of increasing exposure. Because dimensions were determined only to 0.1 mm, measured dimensional changes were noted for only two vanadium samples.

The unalloyed vanadium samples were severely pitted after exposure, and their diameters were reduced as much as 2 mm. The larger weight loss is equivalent to approximately 50% of the initial sample weight. After being removed and cleaned, the vanadium alloys had a lustrous black coating. The metal weight losses observed were equivalent to a loss of 2 mils (0.002 in.) or less, which was too small to be detected directly by the methods used in this program.

In tests outside the reactor, vanadium-titanium binary alloys and vanadium-titanium-chromium ternary alloys have invariably formed hardened layers on the surfaces when exposed at elevated temperatures[5] to sodium containing traces of oxygen or carbon. The ternary alloys have behaved similarly to binary alloys of the same titanium content. In these EBR-II exposures, some of the vanadium alloys indicated in Table VIII did not exhibit a hardened layer after exposure.

The presence of a hardened layer is important because of possible deleterious effects on mechanical properties, particularly on thin sections, i.e., fuel-element jacketing. Possible reasons for the absence of a hardened layer on reactor-exposed samples have been discussed,[6] but no explanation for the variable behavior has been offered.

About half the stainless steel, other iron-base alloy, and nickel-alloy samples experienced weight changes of 0.05 mg/cm^2 or less, which is well within experimental error. Only specimens exposed in capsules TVMV-1 and NMP-1 of subassembly X015 had weight losses definitely beyond the range of experimental error (a weight change of 1 mg is equivalent to 0.18 mg/cm^2) and large enough to cause concern.

Optical metallography has indicated a few areas of slight surface roughness in the Type 304 stainless steel sample A1 in capsule TVMV-1. However, examination with the electron microprobe has shown no change in composition at the surface.

Table VIII shows that the vanadium alloys exposed in capsule NMP-1 also had abnormally high weight losses. The samples in these two capsules were somewhat more difficult to remove from the supporting rod than was usual, but this probably cannot account for the large material losses.

The exposure period of subassembly X015 overlapped that of the other four subassemblies containing corrosion samples. Thus, changes in sodium quality were probably not responsible for the results observed. For an appreciable part of the exposure, the temperature appeared to have been higher than reported. However, results cannot be explained with any high degree of certainty.

Samples of Type 304 stainless steel, Hastelloy-X, Inconel 600, and Multimet were examined with the electron microprobe for changes in surface composition. The Incoloy 800 showed a decrease in chromium concentration at the surface. Inconel 600 showed chromium and nickel depletion at the surface. The other materials were unchanged.

2. Nickel Subassembly

A search of the corrosion literature failed to provide assurance that unclad nickel or chromium-plated nickel subassemblies could be used safely as reflectors in the EBR-II primary sodium. The basic difficulty was that mass-transport phenomena were understood poorly in a quantitative sense, and no reported test had closely approximated the exposure conditions in the reactor.

Two full-size test subassemblies were prepared; these consisted of 30 carefully weighed nickel rings stacked on a solid nickel bar to provide gamma heating and sodium flow equivalent to the actual reflector design. The sodium temperature varied from 700°F at the inlet to 940°F at the outlet, with a flow of 1.2 gpm. The first of these subassemblies has been evaluated after an exposure of 58 days at power (2910 MWd). The second will be examined after approximately one year of exposure.

Table X presents the results of the first exposure. Individual weight losses varied somewhat from specimen to specimen, probably because of handling and cleaning difficulties, but all weight losses were low.

TABLE X. Weight Loss of Nickel-200 Rings[a] Exposed 2910 MWd in Position 7F5

Ring No.	Weight Loss, mg/cm^2	Ring No.	Weight Loss, mg/cm^2
(Top) 1	0.061	16[b]	0.024
2	0.065	17	0.030
3	0.049	18	0.014
4	0.062	19	0.026
5[b]	0.019	20	0.036
6	0.044	21	0.028
7	0.044	22[b]	0.053
8	0.059	23	0.035
9	0.051	24	0.067
10[b]	0.007	25	0.011
11	No data	26	0.041
12	0.027	27	0.026
13	0.050	28[b]	0.020
14	No data	29	0.021
15	No data	(Bottom) 30	c

[a]Rings 2.16 in. OD x 2 in. long; 88 cm^2 exposed to sodium flowing at 1.2 gpm.

[b]Chromium-plated ring.

[c]Because the bottom ring was so badly scratched after the experiment, the weight change could not be considered accurate.

The average loss of the four specimens at the top of the subassembly (~940°F) was 0.06 mg/cm^2; the average of the first four weighable specimens near the bottom (~700°F) was 0.02 mg/cm^2. The maximum weight change corresponded to somewhat less than 3 μin. of uniform nickel loss.

Chromium plating reduced the weight loss. However, the weight changes were so close to the experimental error that the effect of temperature on weight loss for the plated rings was not immediately apparent.

IV. DISCUSSION

The failures of reactor components described were shown to be related to existing flaws and/or to external contamination rather than to deterioration of normally compatible materials. The poor microstructure of the cladding of fuel element C-249-16 and the cracking of the secondary rupture disc were associated with carbonaceous contamination; the bellows failure and the cracking of a thin-section roll pin appeared to be the result of flaws present before insertion into the reactor system. The coolant apparently played a minor role in the development of these failures, beyond providing the high-temperature conditions. However, after the initial penetration of the bellows or rupture disc, the presence of sodium oxide and sodium hydroxide contributed to the further deterioration of the component.

Considering the complexity of the reactor system, the failure rate has been low. The current comprehensive quality-assurance program instituted in the EBR-II Project should assist in maintaining this low rate.

A. Components

An examination of components removed from the reactor indicated that their interaction with the sodium coolant was extremely small at the tank temperature of 700°F and was limited to a slight dissolution of the stainless steel at the higher temperatures.

The only optically observable microstructural change that occurred during the irradiation of the Type 304L stainless steel cladding and the subsequent sodium-removal operation was sensitization (precipitation of carbides at the grain boundaries). Observation of many transverse sections of spent fuel elements further indicated that the degree of sensitization was a function of both the operating temperature and the original carbon concentration of the tubing. For those elements operating at a slightly higher-than-normal temperature, the degree of sensitization appeared to be dependent also on the neutron flux, being greatest at the highest flux regions rather than at the highest temperature zone of the element. No discernible corrosive attack was noted at the coolant-cladding interface, even after extended storage in treated water.

Type 304 stainless steel components (guide thimbles and secondary piping) exposed to the sodium coolant for extended periods experienced some dissolution, particularly where grain boundaries intersected the exposed surface. However, this dissolution did not cause any compositional changes near the surface for the major constituents.

The carbon transport between steels of differing carbon activity was inconsequential, probably because of the extremely low carbon-diffusion rate at temperatures near 700°F. The slightly higher-than-normal carbon concentration in the surface of the secondary piping cannot be conclusively attributed to the pickup of carbon from the sodium, because this increased carbon concentration may have resulted from carbon contamination during the heat treatment of the piping by the supplier.

From the limited data available, no discernible increase in direct sodium attack seemed to be caused by the high radiation level within the core of the reactor. The slight attack on the guide thimbles was related to the temperature and showed no correlation with total fluence.

B. Corrosion Evaluations

The spool-specimen experiments were aimed primarily at demonstrating that vanadium alloys would not deteriorate hopelessly in a large sodium-cooled reactor, even with cold-trap control of the impurity level of the sodium. In that sense, the experiment was successful. Only the unalloyed vanadium was severely attacked. The three alloys lost weight in direct proportion to the time and the temperature of exposure. The limited available data indicated that V-40 wt % Ti and V-15 wt % Ti-7.5 wt % Cr were noticeably more corrosion-resistant than was V-20 wt % Ti in the rapidly flowing sodium. The weight loss of the better alloys was equivalent to uniform penetrations of substantially less than 10^{-3} in. for their exposures of over 100 effective full-power days (time in primary tank of up to 15 months).

Most of the iron-base and nickel-base alloys showed trivial weight changes during their long exposure to the flowing sodium. The exceptions were those specimens in subassembly X015. For an appreciable part of the exposure, the actual temperature of that subassembly appeared to have been much higher than the calculated value. Two vanadium-alloy specimens in this subassembly also experienced somewhat more weight loss than would be expected from a linear extrapolation of other data.

The nickel specimen and the chromium-plated specimens in the special test assembly experienced very slight attack and led to a recommendation to proceed with unclad nickel as a reflector material for the EBR-II.

The small number of coolant-compatibility problems experienced in the operation of EBR-II generates optimism for the LMFBR concept. Although

no direct reference has been made to the surveillance of all the materials listed in Table I, a continuing program of examinations[1] has indicated no significant deterioration of any reactor materials, other than those described in this report.

ACKNOWLEDGMENTS

We gratefully acknowledge the assistance of many of the EBR-II operating personnel in obtaining the specimens described in this report.

We especially thank D. W. Cissel for his many helpful suggestions and D. M. Cheney, B. J. Kestel, and W. D. Jackson for their assistance in preparing the radioactive specimens. The final resolution of failure examinations frequently depended on the skillful application of the electron-beam microprobe by J. E. Sanecki; and C. F. Cheng contributed to the examination of the spool-corrosion specimens.

REFERENCES

1. S. Greenberg, *The EBR-II Materials-surveillance Program: I. Program and Results of SURV-1*, ANL-7624 (Sept 1969).
2. B. D. Holt, *Glovebox Amalgamation for the Determination of Oxygen in Alkali Metals*, ANL-7123 (Dec 1965).
3. C. C. Miles, *An Oxyacidic Flux Method for the Determination of Carbon in Sodium*, Anal. Chem. *41*, 1041 (June 1969).
4. B. D. Holt, *Determination of Hydrogen in Alkali Metals by Isotope Dilution Method*, Anal. Chem. *31*, 51 (Jan 1959).
5. D. F. Atkins, *Mechanical Behavior of Type 304 Stainless Steel in Copper-Contaminated Sodium in the Range 950-1300°F*, AI-AEC-12788 (April 1, 1969).
6. W. H. Olson, C. C. Miles, and D. W. Cissel, "Impurities in EBR-II Sodium and Cover-gas," in *Proceedings of the International Conference on Sodium Technology and Large Fast Reactor Design, November 7-9, 1968*, ANL-7520, Part I, pp. 222-226.
7. D. C. Cutforth, V. G. Eschen, and R. V. Strain, *Post-irradiation Examination of EBR-II Tantalum-clad Antimony Source*, ANL report (to be published).
8. W. E. Ruther, T. D. Claar, and S. Matras, *The Attack on the Cladding of EBR-II Driver Fuel Element C-249-16*, ANL-7537 (March 1969).
9. E. G. Brush, *Construction Materials for Liquid Sodium Systems*, Corrosion *11*, p. 299t (1955).
10. International Nickel Company, Inc., *Engineering Properties of Inconel Alloy 600*, Technical Bulletin T-7, p. 17 (1964).
11. *Metals Handbook*, Vol. I, 8th Edition, p. 417 (1961).
12. D. M. Cheney, Argonne National Laboratory, personal communication (Jan. 30, 1969).
13. C. A. Zimmerman and D. W. Rhodes, *Integrity of Stainless Steel Cladding on EBR-II Fuel in Water*, IN-1331 (Oct 1969).
14. R. Carlander, S. D. Harkness, F. L. Yaggee, and C. F. Cheng, *The Effects of Fast-neutron Irradiation on Tensile Properties and Microstructure of AISI Type 304 Stainless Steel*, ANL report (to be published).
15. S. Greenberg, W. E. Ruther, and H. A. Levin, "Corrosion of Vanadium-Base Alloys in Sodium at 550° to 750°C," in *Symposium on Alkali Metal Coolants*, pp. 63-84, IAEA, Vienna (1967).
16. W. E. Ruther, *The Corrosion of Vanadium and Vanadium-base Alloys in Sodium*, ANL-7505 (May 1969).
17. S. Greenberg, C. F. Cheng, and W. E. Ruther, *In-Reactor Sodium Corrosion of Vanadium and Vanadium-Titanium Alloys*, Nucl. Appl. *4*, pp. 170-172 (March 1968).

ARGONNE NATIONAL LAB WEST
3 4444 00007885 7

ARGONNE NATIONAL LAB WEST
3 4444 00007885 7

ARGONNE NATIONAL LAB WEST
3 4444 00007885 7

ARGONNE NATIONAL LAB WEST
3 4444 00007885 7

ARGONNE NATIONAL LAB WEST
3 4444 00007885 7

ARGONNE NATIONAL LAB WEST
3 4444 00007885 7

ARGONNE NATIONAL LAB WEST
3 4444 00007885 7

ARGONNE NATIONAL LAB WEST
3 4444 00007885 7

ARGONNE NATIONAL LAB WEST
3 4444 00007885 7

ARGONNE NATIONAL LAB WEST
3 4444 00007885 7